Research Article | Vol. 26, No. 6 | 19 Mar 2018 | OPTICS EXPRESS A240
Optics EXPRESS

Optical enhancement of a printed organic tandem solar cell using diffractive nanostructures

JAN A. MAYER,[1] TON OFFERMANS,[1,*] MAREK CHRAPA,[1] MARTIN PFANNMÖLLER,[2,3] SARA BALS,[2] ROLANDO FERRINI,[1] AND GIOVANNI NISATO[1]

[1]*CSEM, Center Muttenz, Tramstrasse 99, 4132 Muttenz, Switzerland*
[2]*Electron Microscopy for Materials Research (EMAT), University of Antwerp, Groenenborgerlaan 171, B-2020 Antwerp, Belgium*
[3]*Presently at the Centre for Advanced Materials, Heidelberg University, Im Neuenheimer Feld 225, 69120 Heidelberg, Germany*
[*]*ton.offermans@csem.ch*

Abstract: Solution processable organic tandem solar cells offer a promising approach to achieve cost-effective, lightweight and flexible photovoltaics. In order to further enhance the efficiency of optimized organic tandem cells, diffractive light-management nanostructures were designed for an optimal redistribution of the light as function of both wavelength and propagation angles in both sub-cells. As the fabrication of these optical structures is compatible with roll-to-roll production techniques such as hot-embossing or UV NIL imprinting, they present an optimal cost-effective solution for printed photovoltaics. Tandem cells with power conversion efficiencies of 8-10% were fabricated in the ambient atmosphere by doctor blade coating, selected to approximate the conditions during roll-to-roll manufacturing. Application of the light management structure onto an 8.7% efficient encapsulated tandem cell boosted the conversion efficiency of the cell to 9.5%.

© 2018 Optical Society of America under the terms of the OSA Open Access Publishing Agreement

OCIS codes: (350.6050) Solar energy; (050.1950) Diffraction gratings; (310.6628) Subwavelength structures, nanostructures; (310.6845) Thin film devices and applications; (310.4165) Multilayer design; (220.4241) Nanostructure fabrication.

References and links

1. W. Clemens, D. Lupo, K. Hecker, and S. Breitung, *OE-A Roadmap for Organic and Printed Electronics*, (Organic and Printed Electronics Association, 2015)
2. M. Hosel, H. F. Dam, and F. C. Krebs, "Development of Lab-to-Fab Production Equipment Across Several Length Scales for Printed Energy Technologies, Including Solar Cells," Energy Technol. (Weinheim) **3**(4), 293–304 (2015).
3. S.-H. Bae, H. Zhao, Y.-T. Hsieh, L. Zuo, N. D. Marco, Y. S. Rim, G. Li, and Y. Yang, "Printable Solar Cells from Advanced Solution-Processible Materials," Chem **1**(2), 197–219 (2016).
4. S. Berny, N. Blouin, A. Distler, H.-J. Egelhaaf, M. Krompiec, A. Lohr, O. R. Lozman, G. E. Morse, L. Nanson, A. Pron, T. Sauermann, N. Seidler, S. Tierney, P. Tiwana, M. Wagner, and H. Wilson, "Solar Trees: First Large-Scale Demonstration of Fully Solution Coated, Semitransparent, Flexible Organic Photovoltaic Modules," Adv Sci (Weinh) **3**(5), 1500342 (2016).
5. W. Zhao, D. Qian, S. Zhang, S. Li, O. Inganäs, F. Gao, and J. Hou, "Fullerene-Free Polymer Solar Cells with over 11% Efficiency and Excellent Thermal Stability," Adv. Mater. **28**(23), 4734–4739 (2016).
6. J. Zhao, Y. Li, G. Yang, K. Jiang, H. Lin, H. Ade, W. Ma, and H. Yan, "Efficient organic solar cells processed from hydrocarbon solvents," Nat. Energy **1**(2), 15027 (2016).
7. N. Li, D. Baran, G. D. Spyropoulos, H. Zhang, S. Berny, M. Turbiez, T. Ameri, F. C. Krebs, and C. J. Brabec, "Environmentally Printing Efficient Organic Tandem Solar Cells with High Fill Factors: A Guideline Towards 20% Power Conversion Efficiency," Adv. Energy Mater. **4**(11), 1400084 (2014).
8. J. Y. Kim, K. Lee, N. E. Coates, D. Moses, T.-Q. Nguyen, M. Dante, and A. J. Heeger, "Efficient Tandem Polymer Solar Cells Fabricated by All-Solution Processing," Science **317**(5835), 222–225 (2007).
9. J. Gilot, M. M. Wienk, and R. A. J. Janssen, "Optimizing Polymer Tandem Solar Cells," Adv. Mater. **22**(8), E67–E71 (2010).

#318375 https://doi.org/10.1364/OE.26.00A240
Journal © 2018 Received 26 Dec 2017; revised 3 Feb 2018; accepted 9 Feb 2018; published 26 Feb 2018

Optics EXPRESS

10. Y. Liu, C.-C. Chen, Z. Hong, J. Gao, Y. M. Yang, H. Zhou, L. Dou, G. Li and Y. Yang, "Solution-processed small-molecule solar cells: breaking the 10% power conversion efficiency," Sci. Rep. **3**, 3356(2013).
11. H. Zhou, Y. Zhang, C.-K. Mai, S. D. Collins, G. C. Bazan, T.-Q. Nguyen, and A. J. Heeger, "Polymer Homo-Tandem Solar Cells with Best Efficiency of 11.3%," Adv. Mater. **27**(10), 1767–1773 (2015).
12. M. Prosa, M. Tessarolo, M. Bolognesi, T. Cramer, Z. Chen, A. Facchetti, B. Fraboni, M. Seri, G. Ruani, and M. Muccini, "Efficient and Versatile Interconnection Layer by Solvent Treatment of PEDOT:PSS Interlayer for Air-Processed Organic Tandem Solar Cells," Adv. Mater. Interfaces **3**(23), 1600770 (2016).
13. J. Hanisch, T. Wahl, C. D. Wessendorf, and E. Ahlswede, "Efficient polymer tandem modules and solar cells by doctor blading," J. Mater. Chem. A Mater. Energy Sustain. **4**(13), 4771–4775 (2016).
14. N. Li and C. J. Brabec, "Air-processed polymer tandem solar cells with power conversion efficiency exceeding 10%," Energy Environ. Sci. **8**(10), 2902–2909 (2015).
15. F. Guo, N. Li, V. V. Radmilović, V. R. Radmilović, M. Turbiez, E. Spiecker, K. Forberich, and C. J. Brabec, "Fully printed organic tandem solar cells using solution-processed silver nanowires and opaque silver as charge collecting electrodes," Energy Environ. Sci. **8**(6), 1690–1697 (2015).
16. J. Tong, S. Xiong, Y. Zhou, L. Mao, X. Min, Z. Li, F. Jiang, W. Meng, F. Qin, T. Liu, R. Ge, C. Fuentes-Hernandez, B. Kippelen, and Y. Zhou, "Flexible all-solution-processed all-plastic multijunction solar cells for powering electronic devices," Mater. Horiz. **3**(5), 452–459 (2016).
17. L. Mao, J. Tong, S. Xiong, F. Jiang, F. Qin, W. Meng, B. Luo, Y. Liu, Z. Li, Y. Jiang, C. Fuentes-Hernandez, B. Kippelen, and Y. Zhou, "Flexible large-area organic tandem solar cells with high defect tolerance and device yield," J. Mater. Chem. A Mater. Energy Sustain. **5**(7), 3186–3192 (2017).
18. T. R. Andersen, H. F. Dam, M. Hosel, M. Helgesen, J. E. Carle, T. T. Larsen-Olsen, S. A. Gevorgyan, J. W. Andreasen, J. Adams, N. Li, F. Machui, G. D. Spyropoulos, T. Ameri, N. Lemaitre, M. Legros, A. Scheel, D. Gaiser, K. Kreul, S. Berny, O. R. Lozman, S. Nordman, M. Valimaki, M. Vilkman, R. R. Sondergaard, M. Jorgensen, C. J. Brabec, and F. C. Krebs, "Scalable, ambient atmosphere roll-to-roll manufacture of encapsulated large area, flexible organic tandem solar cell modules," Energy Environ. Sci. **7**(9), 2925–2933 (2014).
19. J. D. Myers, W. Cao, V. Cassidy, S.-H. Eom, R. Zhou, L. Yang, W. You, and J. Xue, "A universal optical approach to enhancing efficiency of organic-based photovoltaic devices," Energy Environ. Sci. **5**(5), 6900 (2012).
20. Y. Park, J. Berger, Z. Tang, L. Müller-Meskamp, A. F. Lasagni, K. Vandewal, and K. Leo, "Flexible, light trapping substrates for organic photovoltaics," Appl. Phys. Lett. **109**(9), 093301 (2016).
21. S. Esiner, T. Bus, M. M. Wienk, K. Hermans, and R. A. J. Janssen, "Quantification and Validation of the Efficiency Enhancement Reached by Application of a Retroreflective Light Trapping Texture on a Polymer Solar Cell," Adv. Energy Mater. **3**(8), 1013–1017 (2013).
22. C. Cho, H. Kim, S. Jeong, S.-W. Baek, J.-W. Seo, D. Han, K. Kim, Y. Park, S. Yoo, and J.-Y. Lee, "Random and V-groove texturing for efficient light trapping in organic photovoltaic cells," Sol. Energy Mater. Sol. Cells **115**, 36–41 (2013).
23. J. Mayer, B. Gallinet, T. Offermans, and R. Ferrini, "Diffractive nanostructures for enhanced light-harvesting in organic photovoltaic devices," Opt. Express **24**(2), A358–A373 (2016).
24. A. Mertens, J. Mescher, D. Bahro, M. Koppitz, and A. Colsmann, "Understanding the angle-independent photon harvesting in organic homo-tandem solar cells," Opt. Express **24**(10), A898–A906 (2016).
25. G. Dennler, K. Forberich, M. C. Scharber, C. J. Brabec, I. Tomiš, K. Hingerl, and T. Fromherz, "Angle dependence of external and internal quantum efficiencies in bulk-heterojunction organic solar cells," J. Appl. Phys. **102**(5), 054516 (2007).
26. Z. Tang, A. Elfwing, J. Bergqvist, W. Tress, and O. Inganäs, "Light Trapping with Dielectric Scatterers in Single- and Tandem-Junction Organic Solar Cells," Adv. Energy Mater. **3**(12), 1606–1613 (2013).
27. Z. Tang, W. Tress, and O. Inganäs, "Light trapping in thin film organic solar cells," Mater. Today **17**(8), 389–396 (2014).
28. M. Riede, C. Uhrich, J. Widmer, R. Timmreck, D. Wynands, G. Schwartz, W.-M. Gnehr, D. Hildebrandt, A. Weiss, J. Hwang, S. Sundarraj, P. Erk, M. Pfeiffer, and K. Leo, "Efficient Organic Tandem Solar Cells based on Small Molecules," Adv. Funct. Mater. **21**(16), 3019–3028 (2011).
29. D. Cheynsa, B. P. Rand, B. Verreet, J. Genoe, J. Poortmans, and P. Heremans, "The angular response of ultrathin film organic solar cells," Appl. Phys. Lett. **92**(24), 243310 (2008).
30. A. Meyer and H. Ade, "The effect of angle of incidence on the optical field distribution within thin film organic solar cells," J. Appl. Phys. **106**(11), 113101 (2009).
31. J. Mescher, A. Mertens, A. Egel, S. W. Kettlitz, U. Lemmer, and A. Colsmann, "Illumination angle and layer thickness influence on the photo current generation in organic solar cells: A combined simulative and experimental study," AIP Adv. **5**(7), 077188 (2015).
32. N. Kooy, K. Mohamed, L. T. Pin, and O. S. Guan, "A review of roll-to-roll nanoimprint lithography," Nanoscale Res. Lett. **9**(1), 320 (2014).
33. C.-C. Chueh, K. Yao, H.-L. Yip, C.-Y. Chang, Y.-X. Xu, K.-S. Chen, C.-Z. Li, P. Liu, F. Huang, Y. Chen, W.-C. Chen, and A. K.-Y. Jen, "Non-halogenated solvents for environmentally friendly processing of high-performance bulk-heterojunction polymer solar cells," Energy Environ. Sci. **6**(11), 3241 (2013).
34. B. J. T. Villers, K. A. O'Hara, D. P. Ostrowski, P. H. Biddle, S. E. Shaheen, M. L. Chabinyc, D. C. Olson, and N. Kopidakis, "Removal of Residual Diiodooctane Improves Photostability of High-Performance Organic Solar Cell Polymers," Chem. Mater. **28**(3), 876–884 (2016).

Optics EXPRESS

35. J. Huang, J. H. Carpenter, C.-Z. Li, J.-S. Yu, H. Ade, and A. K.-Y. Jen, "Highly Efficient Organic Solar Cells with Improved Vertical Donor-Acceptor Compositional Gradient Via an Inverted Off-Center Spinning Method," Adv. Mater. **28**(5), 967–974 (2016).
36. S. Kouijzer, S. Esiner, C. H. Frijters, M. Turbiez, M. M. Wienk, and R. A. J. Janssen, "Efficient inverted tandem polymer solar cells with a solution processed recombination layer," Adv. Energy Mater. **2**(8), 945–949 (2012).
37. Fluxim, "SETFOS", *https://www.fluxim.com/setfos-intro*
38. M. Pfannmöller, H. Heidari, L. Nanson, O. R. Lozman, M. Chrapa, T. Offermans, G. Nisato, and S. Bals, "Quantitative Tomography of Organic Photovoltaic Blends at the Nanoscale," Nano Lett. **15**(10), 6634–6642 (2015).
39. H. V. Wolferen and L. Abelmann, "Laser Interference Lithography," *Vols. Lithography: Principles, Processes and Materials,* T. C. Hennessy, (Ed., Nova Science Pub Inc, 2011), 133–148.
40. S. B. Dkhil, M. Pfannmöller, S. Bals, T. Koganezawa, N. Yoshimoto, D. Hannani, M. Gaceur, C. Videlot-Ackermann, O. Margeat, and J. Ackermann, "Square-Centimeter-Sized High-Efficiency Polymer Solar Cells: How the Processing Atmosphere and Film Quality Influence Performance at Large Scale," Adv. Energy Mater. **6**(13), 1600290 (2016).
41. R. Timmreck, T. Meyer, J. Gilot, H. Seifert, T. Mueller, A. Furlan, M. Wienk, D. Wynands, J. Hohl-Ebinger, W. Warta, R. A. J. Janssen, M. Riede, and K. Leo, "Characterization of tandem organic solar cells," Nat. Photonics **9**(8), 478–479 (2015).
42. D. Bahro, M. Koppitz, and A. Colsmann, "Tandem organic solar cells revisited," Nat. Photonics **10**(6), 354–355 (2016).
43. D. Bahro, M. Koppitz, A. Mertens, K. Glaser, J. Mescher, and A. Colsmann, "Understanding the External Quantum Efficiency of Organic Homo-Tandem Solar Cells Utilizing a 3-Terminal Device Architecture," Adv. Energy Mater. **5**(22), 1501019 (2015).
44. J. Gilot, M. M. Wienk, and R. A. J. Janssen, "Optimizing Polymer Tandem Solar Cells," Adv. Mater. **22**(8), E67–E71 (2010).

1. Introduction

Solution processable solar cells promise a route to fabricate lightweight and flexible photovoltaics with conventional printing techniques [1]. Well-established large-area methods, like roll-to-roll coating enable an enormous reduction of manufacturing costs and pave the way to integrated off-grid solar harvesting in various devices. Polymer solar cells thereby are considered a good candidate [2, 3] and have already been proven to be compatible with these mass manufacturing techniques [4].

Whereas record efficiencies in single-junction OPV cells have recently reached a power conversion efficiency (PCE) of 11% [5, 6], the use of the tandem concept promises to almost double this value [7] and to achieve PCEs in the order of 20%. This originates from a complementary and thus wider spectral coverage, and a reduction of thermalization losses in the case of hetero tandems [8, 9]. In the case of homo tandems [10, 11] the stack of two thin absorbers of the same material enables a more effective charge extraction with an optical density [8, 10] that is comparable to a single thick active layer.

Despite an additional number of functional layers in the tandem stack compared to single junction cells, tandem cells can be efficiently printed by up-scalable techniques with only the electrodes evaporated [12, 13], whereby a PCE in excess of 10% has recently been reported [14]. Even fully printed, rigid [15] and flexible [16, 17] devices reach efficiencies around 6%. With the first demonstration of roll-to-roll manufactured modules by Andersen et al. [18], the up-scalability of this technology was proven convincingly.

The use of additional optical structures on the surface of organic solar cells can give rise to a further increase of the cell efficiency [19–22] originating from the redirection of incident light into steep propagation angles [23–25]. However, reports on the application of such external light management to tandem devices are still rare [26, 27], which may be based on the observation of a rather angle independent performance in organic tandem cells [28]. Since this effect is based on the complementary angle dependent spectral responses of the sub-cells [24], only a wavelength dependent light management strategy can provide an improved optical field distribution inside the devices, which can be provided by diffractive nanostructures [29–31]. As demonstrated recently, dielectric gratings can be used to couple the incident light into these higher order propagation modes and enhance the conversion efficiency [23]. Consequently, our approach is not dependent on the absorption spectrum of

the organic semiconductor but only linked to the device architecture, i.e. the multilayer tandem stack, which defines the interference conditions. Moreover, the fabrication of these optical structures is compatible with roll-to-roll production techniques such as hot-embossing or UV NIL imprinting, thus making them an optimal cost-effective solution for printed photovoltaics [32].

In this work, we present a homo-tandem cell with all layers coated from non-halogenated solvents [33] in ambient atmosphere using doctor blade coating except for the electrodes. We show that, with this coating method, selected to approximate the conditions during roll to roll manufacturing, high efficiency tandem cells can be obtained in the range of 8-10% with sufficient control over the layer thicknesses to achieve optimized conversion efficiencies in accordance with optical simulation. Next, we demonstrate how diffractive light-management nanostructures can be carefully designed for an optimal redistribution of the light as function of both wavelength and propagation angles in both sub-cells. Applying these structures onto the encapsulated devices boosted the conversion efficiency of the already optimized tandem cells by 8-10%.

2. Design and fabrication of the tandem cell

The tandem cells were fabricated using a PTB7-Th:$PC_{71}BM$ blend in both the front and back layer [Fig. 1]. The PTB7-Th material, (poly[[4,8-bis[(2-ethylhexyl)oxy]benzo[1,2-b:4,5-b′]dithio-phene-2,6-diyl][3-fluoro-2-[(2-ethylhexyl)carbonyl]thieno[3,4-b]thiophenediyl]]), was selected to be used in a homo-tandem as it is a low-band gap material which absorbs until 800 nm with an absorption peak at 700 nm. As poor environmental stability has been reported for PTB7-Th, in particular in combination with diiodooctane (DIO) [14, 34], we opted to process the material from a purely non-halogenated solvent mixture [33]. Because charge transport in the PTB7-Th:$PC_{71}BM$ blend is limited by the thickness [35] – resulting in a substantial reduction of the FF for thickness larger than ~120 nm – it is still possible to achieve a higher efficiency with respect to the single junction cell by using a tandem architecture, as the use of two active layers will allow for enough light to be absorbed, while maintaining a good fill factor (FF). As recombination layers ZnO nanoparticles were used in combination [36] with a pH-neutral formulation of PEDOT:PSS, poly(3,4-ethylenedioxythiophene)-poly(styrenesulfonate) (Orgacon N-1005, provided by AGFA).

The optical stack of the homo-tandem was simulated [Fig. 1] with the commercial software tool SETFOS [37]. The thicknesses of 20 nm and 40 nm were chosen for the ZnO and pH-neutral PEDOT:PSS layer, respectively, based on experimental considerations, as smaller layer thicknesses result in a non-closed recombination layer, while larger thicknesses result in resistive losses. The software was then used to calculate the maximum photocurrent (IQE = 1) generated in both PTB7-Th layers as function of their thickness. Since the subcells are connected serially, the thicknesses of both front and back active layers needs to be tuned such that their photocurrents match, otherwise, one of the subcells would limit the current through the tandem stack. From Fig. 2(a) we conclude that, for a narrow range of 75-95 nm in the thickness of the front active layer, the photocurrent matching conditions are met. The highest matched photocurrents (10.4-10.6 mA/cm^2) are predicted in combination with a 90-110 nm thick back active layer. Assuming an IQE of 80-90% [11] the expected efficiency of such a tandem cell can be calculated to be in the range 8-9%, by using a FF of 60% and twice the V_{oc} of a single junction cell (2 x 0.78 = 1.56 V).

Optics EXPRESS

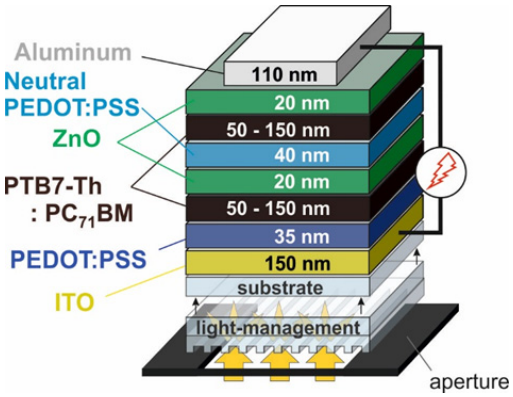

Fig. 1. Stack of the tandem cell with additional light management structure.

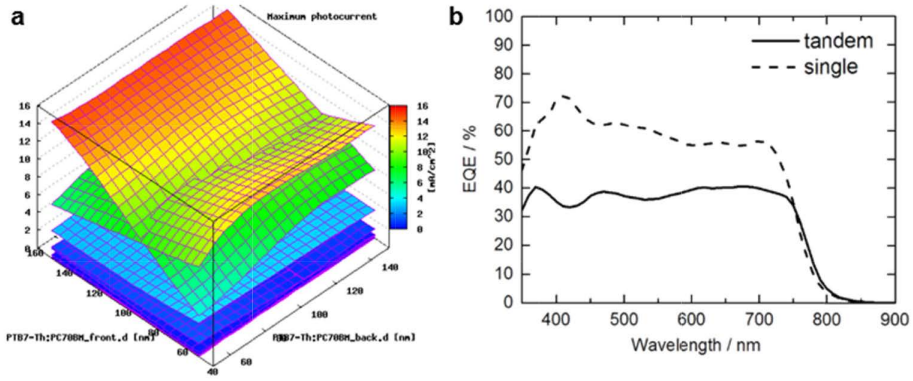

Fig. 2. (a) 2D surface plot of the thickness dependent photocurrent in front and back active layers of the homo-tandem cell. The intersection of the plots represents the thicknesses for photocurrent matching. (b) EQE spectra of the hero tandem device in this work and of a representative single junction device ITO / PEDOT:PSS / PTB7-Th:$PC_{71}BM$ (110 nm) / ZnO / Al.

Analysis of the performance of a series of 57 cells of the printed tandem solar cells (Table 1) shows the feasibility of fabricating solar cells with >8% efficiency with high reproducibility. The higher efficiency of some tandem cells above the average can be explained by an optimal combination of all layer thicknesses, including the charge extraction layers. A small variation in thickness is always present when blade coating an ink at moderate speeds across a substrate; typically, the coated film has a gradient in its thickness, decreasing in the coating direction, which results in a significant spread in results for solar cells on the same substrate. An ultra-thin cross-section for transmission electron microscopy (TEM) was prepared using focused ion beam from an area with maximum efficiency for a specific substrate. Scanning TEM (STEM) was applied on this cross-section in high-angle annular dark-field mode for precise determination of layer thicknesses and in spectroscopic imaging mode to reveal the nanomorphology of all organic layers [37, 39]. The dark-field image in Fig. 3 shows a deviation to the thicknesses in the design stack for the bottom PEDOT:PSS layer (~15 nm), the pH-neutral PEDOT:PSS layer (~10 nm) and the front active layer thicknesses (~70 nm). A new simulation with the updated thicknesses predicts a small mismatch in the photocurrent generation with the front subcell generating less current than the back subcell, with 8.0 mA and 10.8 mA/cm^2, respectively. In order to visualize the organic phases at the nanoscale, spectroscopic imaging was realized by recording low-energy-loss spectra for each scan position. Mapping out peak positions of bulk plasmon excitations

Optics EXPRESS

allows to discriminate polymer-rich, fullerene-rich areas and phases with mixed composition. When comparing the nanomorphologies [Fig. 4(b)] of both front and back subcells, similarly sized fullerene-rich domains are found. Importantly, both subcells are clearly separated by a 10 nm pH-neutral PEDOT:PSS layer which mixes partially with the nanoporous ZnO layer below [38]. Interestingly, the fullerene-rich phase is distributed through the entire thickness of the photoactive layers with a relatively large interface between the bottom PEDOT:PSS layer and the fullerene for hole transport, which may account for lower open circuit voltages observed for the first 5 samples in the set. For the best tandem cells produced a V_{oc} of twice that of a single junction cell was obtained. As the active layers in the tandem consists of the same material, the front subcell acts as a filter to the back subcell, resulting in reduced J_{sc} and EQE [Fig. 2(b)] compared to the single junction. With the doubling of the V_{oc} and a maintained FF, the tandem architecture results in an overall improved performance over the single junction.

Table 1. J-V data of 57 tandem cells on 13 substrates (5 cm x 5 cm). The efficiency reported is the efficiency obtained from J-V measurements under approximate AM1.5g illumination corrected with the J_{sc} obtained by integrating the EQE spectra and convoluting with the AM1.5 solar spectrum. Devices on substrates 1-7 with active areas of 0.24 cm^2 were masked to 0.04 cm^2 during illumination, and devices on substrates 8-13 with active areas of 1.4 cm^2 were masked to 1 cm^2. Values in brackets denote the mean value. The mean efficiency of all 57 cells is 8.1%. Performance data of a representative data set of single junction cells fabricated under identical conditions are included at the end of the table.

Sample	Cell area (cm^2)	number of cells	V_{oc} (V)	J_{sc}^{EQE} (mA/cm^2)	FF (%)	Efficiency (%)
1	0.04	7	1.500 ± 0.003	8.8 ± 0.8	60 ± 4	7.9 ± 0.4
2	0.04	7	1.502 ± 0.005	9.4 ± 0.5	60 ± 0.7	8.5 ± 0.4
3	0.04	7	1.29 ± 0.52	7.4 ± 3.5	53 ± 17	7 ± 3
4	0.04	7	1.50 ± 0.02	9.9 ± 0.4	58 ± 2	8.6 ± 0.7
5	0.04	7	1.478 ± 0.009	8.7 ± 0.5	51 ± 0.8	6.6 ± 0.5
6	0.04	5	1.553 ± 0.003	9.1 ± 0.3	58 ± 3	8.1 ± 0.3
7	0.04	7	1.561 ± 0.009	9.0 ± 0.4	52 ± 3	7.3 ± 0.7
8	1	2	1.573 ± 0.003	8.7 ± 0.1	58 ± 2	8.0 ± 0.3
9	1	2	1.560 ± 0.0001	8.5 ± 0.1	61 ± 1	8.04 ± 0.05
10	1	1	1.563	8.79	61	8.4
11	1	2	1.572 ± 0.001	8.80 ± 0.05	62 ± 0.005	8.60 ± 0.04
12	1	2	1.576 ± 0.002	8.74 ± 0.04	61.0 ± 0.6	8.4 ± 0.1
13	1	1	1.594	8.63	61	8.4
Average tandem		**57**	**1.5 ± 0.2 (1.5)**	**8.9 ± 1.5 (9.1)**	**57 ± 7.5 (59)**	**7.7 ± 1.4 (8.1)**
Average single junction reference			0.78 ± 0.01	14.8 ± 0.7	58 ± 1	6.7 ± 0.3

Optics EXPRESS

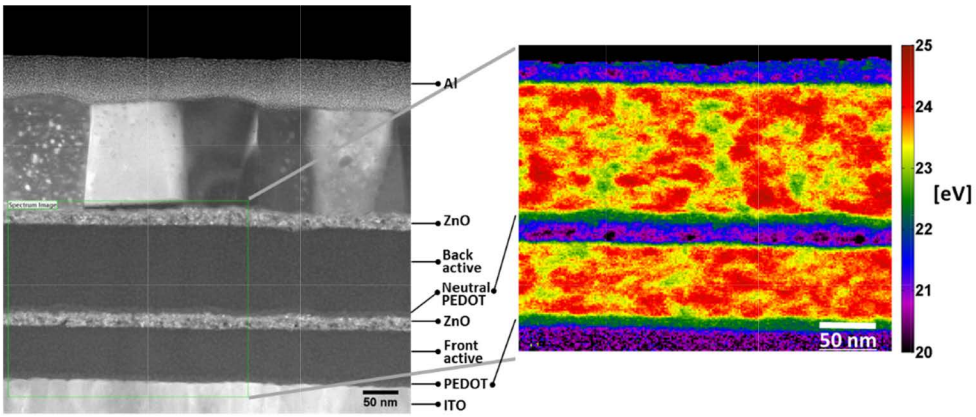

Fig. 3. Dark field STEM image of a focused ion beam cross-section of the tandem cell, with (inset on the right) a selected area where spatially resolved electron energy-loss spectroscopy was applied for mapping of the nanomorphology. Red: fullerene rich; Green: polymer rich; purple: ZnO nanoparticles.

A selection of tandem cells from the series were encapsulated with a glass cover plate, and subsequently characterized independently at CSEM and the Karlsruhe Institute of Technology (KIT) using a solar simulator calibrated with a certified Si reference cell. The cells for this independent characterization were fabricated with a large area (1.4 cm^2), which was masked to exactly 1 cm^2 for the measurement. The best performing cell measured at KIT yielded an efficiency of 8%, with V_{oc} = 1.58 V, J_{sc} = 8.2 mA/cm^2, FF = 62%.

3. Light management

The light management structure was designed as an external surface structure [23]. Such a solution is advantageous as it does not interfere with the production process of the cell itself. The structure may be fabricated on a stand-alone substrate and laminated on a ready-to-use encapsulated device, or directly fabricated on the surface of the substrate.

Simulations of the optical absorbance in the two sub-cells of the optimized tandem stack show that the front sub-cell absorbs more in the red than the back cell, and the back cell more in the green [Fig. 4(a)]. The simulated absorption as function of the light propagation angle in the substrate [Fig. 4(b)] - which is accessible by diffraction at the nanostructured substrate surface [23] – further yields an upper limit (corresponding to IQE = 1) for the angle dependent photocurrent, which is observed to be superior for the back subcell. Since the current is limited by the weaker front subcell, not much improvement can thus be expected by light redirection. However, when regarding the wavelength dependency for both subcells, it can be observed that the angle-dependent absorption is beneficial in different regions for the two subcells. Whereas the front subcell absorption can be enhanced by up to 50% for large diffraction angles in the range of 420-600 nm [Fig. 4(c)], for the back subcell an enhancement is revealed only between 550 and 800 nm [Fig. 4(d)]. For most combinations of wavelength and propagation angle, hence, only one subcell can be improved while the absorption of the other subcell is decreased.

Optics EXPRESS

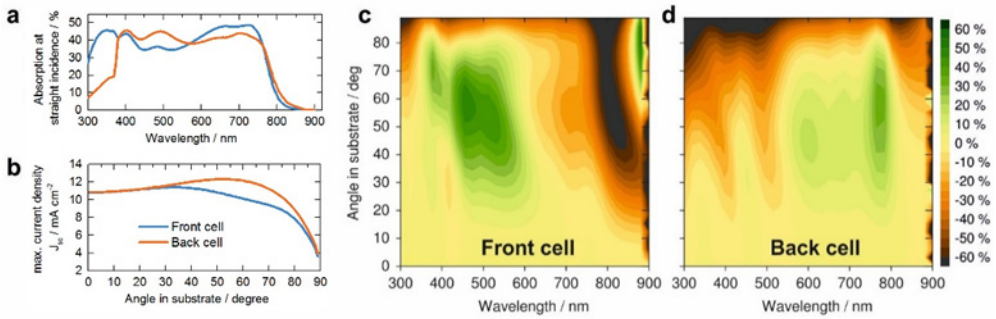

Fig. 4. (a) Simulated absorption of the two subcells in the tandem stack and (b) the respective angle-dependent current generation. (c) Absorption in-/decrease for redirected light for the front subcell and (d) for the back subcell with respect to normal incidence.

However, since the enhancement can be much larger than the losses in the other subcell, a light management nanostructure can be optimized such that its diffraction pattern distributes the light for a best compromise of the two subcells. By these means an overall gain can be obtained if the wavelength integrated absorption is considered. If the lower current of both active layers is taken as a measure and the period and the depth of the nanostructure are varied, simulations suggest an enhancement of 7% for a rectangular nanostructure [Fig. 5(a)] and up to 9% for a Lorentzian shape [Fig. 5(b)] if the nanostructure is attached to the device surface.

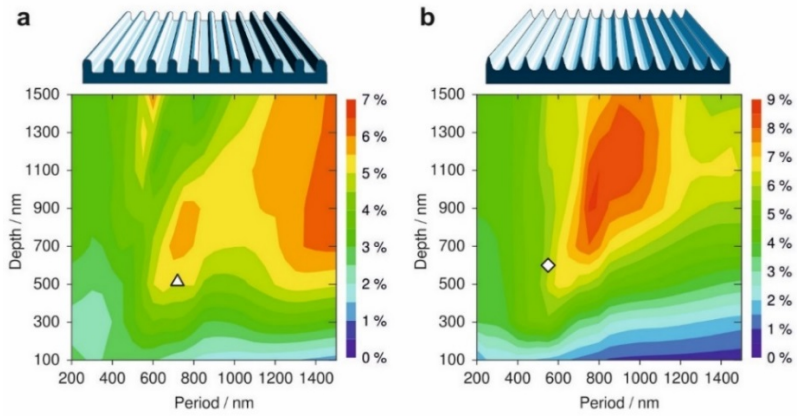

Fig. 5. Simulations of the absorption enhancement in the front active layer with two different light management geometries. (a) Up to 7% increase can be obtained by a periodic nanostructure with a squared profile and (b) up to 9% increase in the absorption can be expected for a Lorentzian shape.

Both nanostructures were fabricated on glass as replicas from the original master. The characterization by SEM [Fig. 6(a) and 6b)] shows a small mismatch to the optimum parameters (indicated by the white triangle and diamond in Fig. 5 for squared and Lorentzian structures, respectively). Despite this displacement, simulations still suggest an enhancement of more than 5% for both structures applied to the tandem.

When laminated to the tandem device with index matching liquid, the current density was enhanced in a successive measurement for both incoupling structures under investigation [Fig. 6(c)]. Moreover, successive measurements on multiple devices with the Lorentzian nanostructure reveal the resulting increase in device efficiency: Fig. 6d shows three measurements on four tandem solar cells (4 mm^2 masked area), where the Lorentzian light management was first laminated to the device, secondly removed and finally laminated a

Optics EXPRESS

second time, still getting back to the 8-10% enhancement in efficiency with respect to the reference measurement without light management.

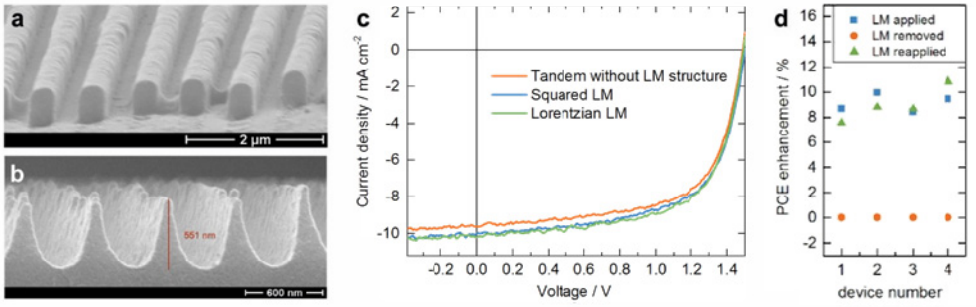

Fig. 6. SEM images of the squared (a) and the Lorentzian (b) shaped periodic nanostructures. (c) Its beneficial effect on the generated current in the tandem device can be recognized in the J-V curve. (d) This increase translates directly onto the device efficiency in multiple devices under test and is reversible, if the structure is removed from the surface and reapplied.

Since this increase is larger than predicted, the results indicate that the currents in the reference tandem solar cell were not matched perfectly. If the chosen nanostructure parameters are compared for the front and back subcells separately, it becomes clear that the chosen structure is more advantageous for the front subcell [Fig. 7]. This suggests that the front subcell was initially a little weaker in the current generation - in accordance with the STEM analysis [Fig. 3] - which was thus compensated by the light management structure.

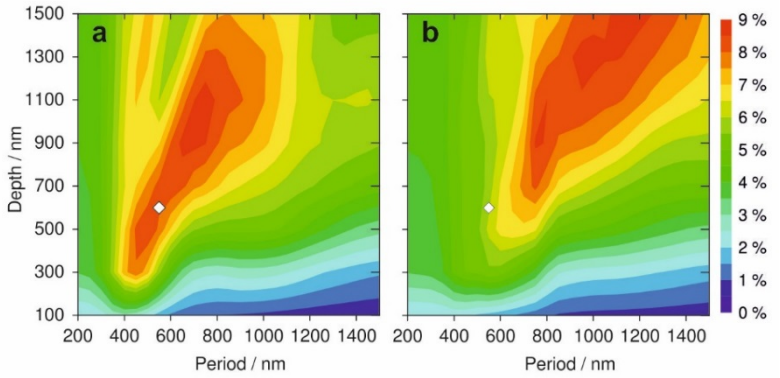

Fig. 7. Simulations of the absorption enhancement with the Lorentzian structure using the parameters updated according to STEM measurements (Fig. 3). (a) >8% increase in the absorbance can be obtained in the front active layer while (b) up to 7% increase in the absorption can be expected for the back active layer.

For the best device [Fig. 8], the efficiency was improved by 9% (relative), from 8.7% to 9.5% (measured at CSEM), which is in line with the relative improvements observed for the other devices [Fig. 6(d)]. The performance of the device with the light management was again verified at KIT, eleven days after fabrication and encapsulation. A reduced V_{oc} (–2.7%) and a slightly lower short circuit current density (–4.3%) yielded a reduced efficiency, but with the relative enhancement effect of the light management still preserved.

Optics EXPRESS

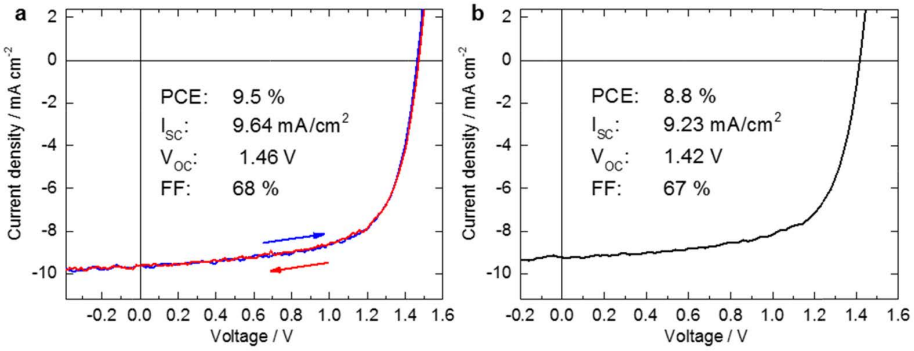

Fig. 8. Hero device measured at CSEM (a) four days after fabrication and at KIT (b) after 11 days for comparison.

4. Conclusions

Homo-tandem cells with efficiencies between 8 and 10% could be produced using a roll-to-roll (R2R) compatible coating method under ambient conditions in air and with the use of non-chlorinated solvents. A light management structure was designed specifically for an optically and electrically optimized homo-tandem solar cell and was fabricated also with R2R compatible methods. Upon lamination of the light management structure the tandem solar cell performance was increased from 8.7% to 9.5%. The improvement results from enhanced absorption, in particular by the current limiting front subcell.

5. Experimental section

5.1. Fabrication of the tandem cells

PEDOT:PSS VP AI4083 (Clevios) was blade coated on pre-patterned ITO coated glass substrates (25 cm^2, Geomatec) and baked at 140°C for 10 minutes in air. The PTB7-Th (1-Material) was mixed with $PC_{71}BM$ (Solenne) in a 1:1.5 ratio in a mixture of o-xylene and 1,2-DMN and stirred overnight at 70°C. The solution was cooled to room temperate and blade coated in air on the substrate kept at 60°C, followed by a first layer of a ZnO nanoparticle formulation (GenesInk), a 1 wt% pH-neutral PEDOT:PSS (low conductivity Orgacon N-1005, AGFA), a second PTB7-Th:$PC_{71}BM$ layer, and a top ZnO layer. The coatings were transferred to a N_2 filled glove box and baked for 20 minutes at 60°C, The coatings were kept in vacuum ($2 \cdot 10^{-6}$ mbar) overnight prior to thermal evaporation of the aluminium top electrode.

5.2. Fabrication of the light management structures

The light management structures used in this work are fabricated by laser interference lithography (LIL) [39], an optical method that enables the creation of large-area one- or two-dimensional periodic nanostructures with different geometries. Once created on a sufficiently large area with LIL, the resulting master structure can be used for repeated soft-embossing of a UV-curable polymer. For replication the grating master is imprinted into an UV-curable polymer which is dispensed on a glass substrate. Exposure with a UV lamp forms a transparent and rigid film, which remains when the master is released. The structured glass plate is reversibly laminated to the light incident side of the tandem cell using an index matching oil.

Optics EXPRESS

5.3. Measurements

The cross-section for STEM imaging was prepared using a Helios Nanolab 650 (Thermo Fisher Scientific). Microscopic investigations were performed with a Titan 60-300 (Thermo Fisher Scientific) equipped with a GIF Enfinium Spectrometer (Gatan) and operated at 120 kV. The scanning step size for spectral imaging was set to 2 nm. The area was not irradiated before spectral imaging except for the dark-field overview image using a very low electron dose. Analysis of STEM spectroscopic imaging data sets was done using HyperSpy, an open-source Python library for analysis of multidimensional data sets (www.hyperspy.org). This includes Lorentzian fits to determine the plasmon peak energies. Further experimental details can be found in [38] and [40].

Layer thicknesses were measured using tactile stylus profiler (Tencor P-10) and an AFM (Park XE-70).

J-V characteristics at CSEM were measured using a Keithley 2400 SMU under the illumination of an Air Mass 1.5 G filtered Xenon lamp with an irradiation intensity of ~70 mW/cm^2. The EQE measurement were performed using a Si photodiode (S1337 Hamamatsu) calibrated by SUPSI (www.supsi.ch). The EQE measurement were performed without light biasing or electrical biasing the subcells in the tandem. A correct characterization of tandem devices requires a more elaborate procedure than performed [41–43]. The spectral responses of both sub-cells deviate even in the homo tandem configuration [Fig. 4(a)] which necessitates the calculation of separate mismatch factors based on the EQE of both sub-cells [44]. Since this requires an advanced measurement setup, a mismatch factor of 1.0534 was estimated using the spectral response of the full device without light management, in order to correct the measurements in Fig. 8.

J-V characteristics at KIT were measured with a Keithley 238 source meter unit under illumination from a spectrally monitored solar simulator (Oriel 300 W, 1000 W/m^2, ASTM AM 1.5g), calibrated by a KG5 filtered silicon reference cell (91150-KG5, Newport).

Funding

FP7 European collaborative project SUNFLOWER (FP7-ICT-2011-7, grant number 287594); German Federal Ministry of Education and Research (BMBF) (03xEK3504, project TAURUS); FP7 European project ESTEEM2 (grant number 312483); HEiKA centre FunTECH-3D.

Acknowledgments

The authors acknowledge Louis-Dominique Kaufmann (GenesInk) for providing the ZnO nano particle ink, Dirk Bollen (AGFA) for the pH neutral PEDOT:PSS formulation. The authors thank Daniel Bahro, Konstantin Glaser and Alexander Colsmann from the Light Technology Institute, Karlsruhe Institute of Technology (KIT) for the independent verification of the solar cell performance. The authors further thank Stéphane Altazin and Beat Ruhstaller (Fluxim) for simulation support.

Disclosures

The authors declare that there are no conflicts of interest related to this article.

148.175.11.111 {ts '2018-09-21 09:42:42'}